JOURNAL OF THEORETICAL AND APPLIED MECHANICS
48, 4, pp. 871-896, Warsaw 2010

APPLICATION OF ARTIFICIAL NEURAL NETWORKS IN PARAMETRICAL INVESTIGATIONS OF THE ENERGY FLOW AND SYNCHRONIZATION

Artur Dąbrowski
Anna Jach
Tomasz Kapitaniak

Technical University of Lodz, Division of Dynamics, Łódź, Poland
e-mail: ar2de@p.lodz.pl; anna.jach@p.lodz.pl; tomaszka@p.lodz.pl

Dynamics of nonlinear systems is a very complicated problem with many aspects to be recognized. Numerous methods are used to investigate such systems. Their careful analysis is connected with long-time simulations. Thus, there is great need for methods that would simplify these processes.
In the paper, an application of Artificial Neural Networks (ANNs) supporting the recognition of the energy flow and the synchronization with use of Impact Maps is introduced. This connection applies an idea of the Energy Vector Space in the system with impacts. An energy flow direction change with the synchronization as a transitional state is shown. A new type of the index allowing one to control the system dynamic state is introduced. Results of the numerical simulations are used in the neural network teaching process. Results of a comparison of the straight impact map simulation and the neural network prediction are shown. Prediction of system parameters for the energy flow synchronization state with use of the neural network is presented.

Key words: nonlinear dynamics, chaos synchronization, artificial neural networks

1. Introduction

Artificial neural networks are nowadays one of the most intensively developing scientific branches. It is related to many interdisciplinary aspects of neural network applications. ANNs are used in robotics, neuroscience, general engineering, chemistry, medicine, financial markets, mechanics, electronics, biocybernetics, automatics, real neural network simulations,informatics, logistic

systems, for image recognition, speech recognition, in optimisation problems, for solving different problems of high complexity and unknown rules (Duch and Pilichowski, 2007; Duch *et al.*, 2000; Dudek-Dyduch *et al.*, 2009; Markiewicz and Ossowski, 2005; Ogiela *et al.*, 2006, 2008; Ossowski *et al.*, 2004, 2005; Szaleniec *et al.*, 2008; Tadeusiewicz *et al.*, 2008; Tadeusiewicz and Ogiela, 2004; Zhang and Sun, 2004). In the paper, ANNs are used as a tool supporting investigations of the coupled oscillating system dynamics. In some aspects, prediction of the dynamical system behaviour with ANNs is similar to energy methods – both can be treated as a black box with some information given as the input and, after realization of some functions in the black box, a result is received as the output. A new method applying an index, based on the idea taken from energy methods, is introduced in the paper. An energy flow as the final effect of external and internal interactions is a very important aspect of the system dynamics, and still arouses much interest in the scientific world (Gourdon and Lamarque, 2005; Hu *et al.*, 2004; Keane and Price, 1991; Kishimoto *et al.*, 1995; Korotkov, 2002; Mace, 1992, 1994; Sado, 1992; Maidanik and Becker, 2003; Tsakirtzis *et al.*, 2005). Different methods are applied to solve problems connected with the energy flow: Statistical Energy Analysis (Hu *et al.*, 2004; Kishimoto *et al.*, 1995; Mace, 1992), Finite Element Method (Hu *et al.*, 2004), mode theory (Sado, 1992). Observations of the system energy state or its part give a possibility to determine and explain the reasons of the system behaviour. It allows one to control the system dynamics, which is especially important in chaotic systems (Dąbrowski and Kapitaniak, 2001, 2009; Kapitaniak, 1996). Such control can cause, for instance, oscillation reduction (Dąbrowski, 2000; Dąbrowski and Kapitaniak, 2001, 2009), giving thus new possibilities of the system application. Simultaneously, systems with coupling and synchronization between coupled systems belong nowadays to the most often investigated phenomena (Astakhov *et al.*, 1999; Blekhman II, 1988; Czołczynski *et al.*, 2009; Fries *et al.*, 2001; Kapitaniak and Maistrenko, 1998; Keane and Price, 1991; Lachaux *et al.*, 2000, 2003; Lindner and Schimansky-Geier, 2000; Mace, 1994; Nichols *et al.*, 2007; Pecora *et al.*, 1997; Rodrigues *et al.*, 1999; Shu *et al.*, 2005; Stefański, 2004; Stefański *et al.*, 2005; Yampi *et al.*, 2007). One of the analyzed coupling types is an impact coupling (Błażejczyk-Okolewska *et al.*, 2001, 2007; Dąbrowski, 2000; Dąbrowski and Kapitaniak, 2009; Kapitaniak and Wiercigroch, 2000; Lee and Yan, 2006; Ma *et al.*, 2008). Because of the discontinuity of such systems, global system dynamics can be recognized analytically only in particular cases (Aidanpaa and Gupta, 1993; Czołczyński, 2001; Peterka, 1970; Peterka and Vacik, 1992). In the paper, a new method of global dynamics analysis of systems with impacts is proposed.

A structure and an application of the Impact Map in investigations of the coupled system dynamics are introduced. This structure applies an idea of the Energy Vector Space (Dąbrowski, 2000, 2005, 2007, 2009) in the system with impacts. An energy flow direction change with synchronization as a transitional state is shown. Results of the numerical simulations are used in the neural network teaching process. A comparison of results of the straight impact map simulation and the neural network prediction is shown. Prediction of system parameters for the energy flow synchronization state with use of the neural network is presented.

2. Method algorithm

A simplified algorithm is shown in Fig. 1. The task for this algorithm was to work out a method that finds a neural network to solve the problem of the energy flow synchronization prediction. Such investigations of the nonlinear system dynamics are very often related to investigations of the control index behaviour. In such cases, a given value of the index is connected with some specific system behaviour. The task is how to find areas of the desired index values. Depending on the system type, different methods can be applied. A bifurcation diagram is most often the supporting tool for such an analysis. However, it is slightly like wandering in the dark. To make stable investigations without introducing disturbances causing unstable motions, or jumping between coexisting attractors, it is required to change slightly tuning of the system coefficient while creating such a diagram. The method is simple but for the global investigations of the whole system parameters with such delicate tuning, one would need much time. A new method that simplifies such an analysis is proposed in the paper. Investigations with a new type of the control index supported by the artificial neural network are introduced. The first step of the system study are numerical simulations and preparation of a teaching set. The teaching set does not have to be very accurate. Thus, a special method to prepare such a set is proposed and this is the clue to the simplification of such an analysis. The idea of this method is presented in Fig. 2. One can see a set of bifurcation diagrams in it. Each line represents one bifurcation diagram and shows the direction of the system parameter changes. Note that unlike the traditional bifurcation diagrams, two system parameters are changed at the same time. Thanks to that it is possible to prepare the set of dispersed data representing the system dynamics with slightly tuning of the system parameters without introducing disturbances causing unstable motions, or jumping

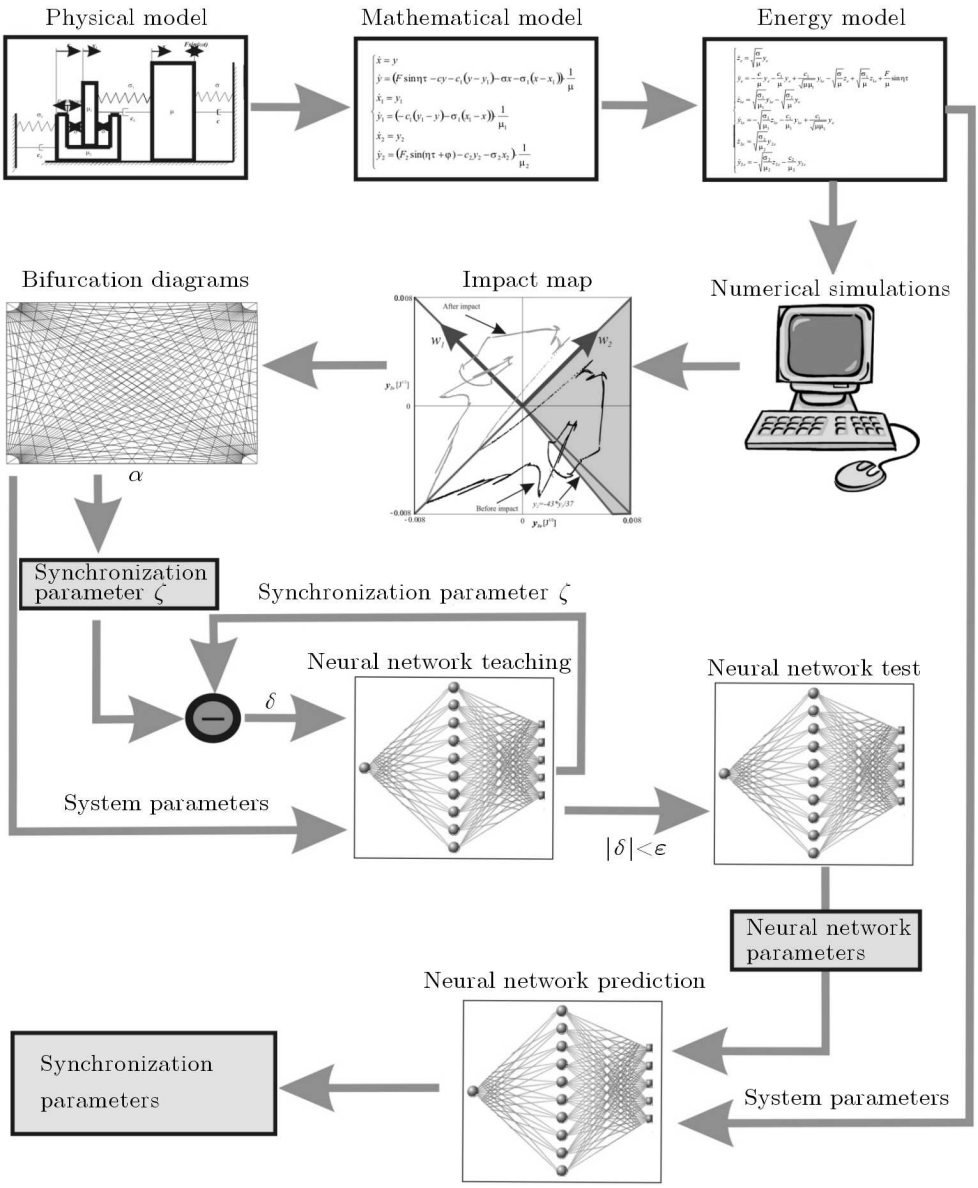

Fig. 1. A simplified algorithm of the proposed method

between coexisting attractors. Preparation of the teaching set was made in Delphi, with the Runge-Kutta method applied to integrate the differential equation set. Then, the teaching set was entered into the Statistica Neural Network software. After the teaching procedure, such a network works as an

approximator, allowing one to find the system control index for the whole system parameter range. To find the desired control index value output, neural network values were examined. In the case under consideration, the desired control index value represents the energy flow synchronization phenomena of coupled systems.

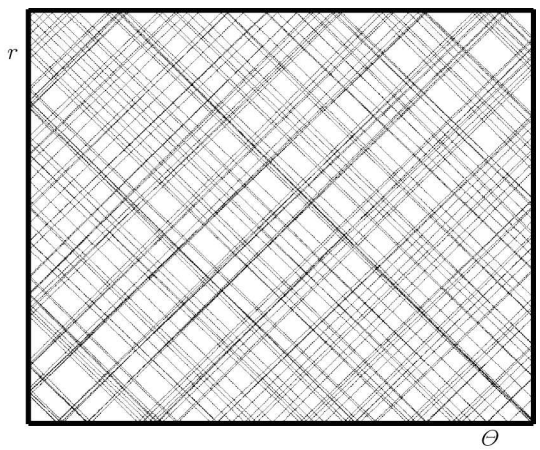

Fig. 2. The set of bifurcation diagrams

3. Introduction to the Impact Map structure and the energy flow analysis

Consider the system shown in Fig. 3. For some ranges of the system parameters, it works as an impact damper of motion of the oscillator μ (Dąbrowski, 2000; Dąbrowski and Kapitaniak, 2001, 2009). The system consists of three oscillators. The external harmonic force excites the oscillator μ. It is joined with the classical dynamical absorber μ_1. This absorber is allowed to collide with the third oscillator μ_2 excited by the second external harmonic force.

In the periods between impacts, the mathematical model of the system is given by six differential equations of the first order

$$\begin{aligned} \dot{x} &= y & \dot{y} &= [F\sin\eta\tau - cy - c_1(y-y_1) - \sigma x - \sigma_1(x-x_1)]\frac{1}{\mu} \\ \dot{x}_1 &= y_1 & \dot{y}_1 &= [-c_1(y_1-y) - \sigma_1(x_1-x)]\frac{1}{\mu_1} \\ \dot{x}_2 &= y_2 & \dot{y}_2 &= [\Theta F\sin(\eta\tau+\varphi) - c_2 y_2 - \sigma_2 x_2]\frac{1}{\mu_2} \end{aligned} \tag{3.1}$$

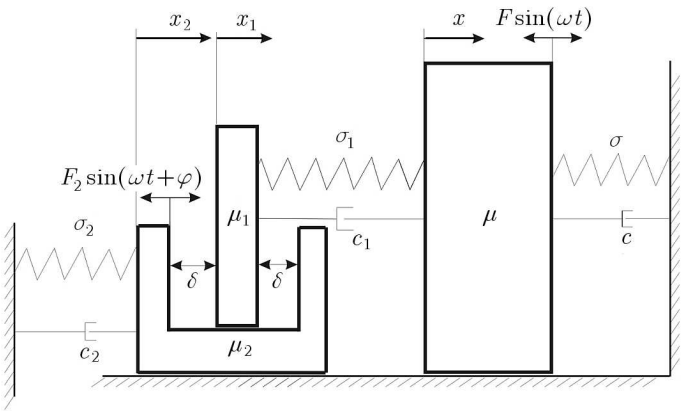

Fig. 3. The physical model of the system

where: μ, μ_1, μ_2 are masses, σ, σ_1, σ_2 – stiffness coefficients of the springs, c, c_1, c_2 – damping coefficients, F – amplitude of the external excitation force acting on μ, F_2 – amplitude of the external excitation force acting on μ_2, ω – frequency of the external excitation force

$$\eta = \frac{\omega}{\alpha} \qquad \tau = \alpha t \qquad \alpha = \sqrt{\frac{\sigma}{\mu}} \qquad \Theta = \frac{F_2}{F} \tag{3.2}$$

The 4-th order Runge-Kutta method is applied to solve this set of differential equations.

The impacts between the dynamical and impact absorbers are entered into the mathematical model over the restitution coefficient r and the momentum equation. The impact point searching algorithm consisted of two stages repeated with a decreasing time step until the distance between impacting oscillators is less than the parameter ε.

- Stage 1 – Searching for the crossing point of the trajectories.
- Stage 2 – Making one step back.

The possibility of motion with impacting oscillators "glued together" was also considered.

The phase vector in the standard phase space $\mathbb{R}^6$ is represented by six components, namely

$$x;\ y;\ x_1;\ y_1;\ x_2;\ y_2 \tag{3.3}$$

Transform the phase space as follows:

1. Instead of the displacement coordinates x, x_1, x_2, take the deflections of the springs.

$$z = x \qquad z_1 = x_1 - x \qquad z_2 = x_2 \tag{3.4}$$

2. Depending on the coefficients σ_i and μ_i, squeeze and stretch the space along the directions of z_i and y_i.

In the following two steps, a new energy space can be obtained.

In the first step, one obtains a new space $\mathcal{V}$ with the basis E

$$E = (\boldsymbol{e}_z, \boldsymbol{e}_y, \boldsymbol{e}_{1z}, \boldsymbol{e}_{1y}, \boldsymbol{e}_{2z}, \boldsymbol{e}_{2y}) \tag{3.5}$$

where

$$\begin{aligned} \boldsymbol{e}_z &= [1,0,0,0,0,0]^\top & \boldsymbol{e}_y &= [0,1,0,0,0,0]^\top \\ \boldsymbol{e}_{1z} &= [0,0,1,0,0,0]^\top & \boldsymbol{e}_{1y} &= [0,0,0,1,0,0]^\top \\ \boldsymbol{e}_{2z} &= [0,0,0,0,1,0]^\top & \boldsymbol{e}_{2y} &= [0,0,0,0,0,1]^\top \end{aligned} \tag{3.6}$$

Change the basis vectors of the space $\mathcal{V}$. Then, the new energy basis E_N of this space is

$$E_N = (\boldsymbol{b}_z, \boldsymbol{b}_y, \boldsymbol{b}_{1z}, \boldsymbol{b}_{1y}, \boldsymbol{b}_{2z}, \boldsymbol{b}_{2y}) \tag{3.7}$$

where

$$\begin{aligned} \boldsymbol{b}_z &= [(\sqrt{\sigma})^{-1},0,0,0,0,0]^\top & \boldsymbol{b}_y &= [0,(\sqrt{\mu})^{-1},0,0,0,0]^\top \\ \boldsymbol{b}_{1z} &= [0,0,(\sqrt{\sigma_1})^{-1},0,0,0]^\top & \boldsymbol{b}_{1y} &= [0,0,0,(\sqrt{\mu_1})^{-1},0,0]^\top \\ \boldsymbol{b}_{2z} &= [0,0,0,0,(\sqrt{\sigma_2})^{-1},0]^\top & \boldsymbol{b}_{2y} &= [0,0,0,0,0,(\sqrt{\mu_2})^{-1}]^\top \end{aligned} \tag{3.8}$$

The transition matrix $\mathbf{A}_{E_N \leftarrow E}$ from the basis E to the basis E_N of the energy space takes the form

$$\mathbf{A}_{E_N \leftarrow E} = \begin{bmatrix} \sqrt{\sigma} & 0 & 0 & 0 & 0 & 0 \\ 0 & \sqrt{\mu} & 0 & 0 & 0 & 0 \\ 0 & 0 & \sqrt{\sigma_1} & 0 & 0 & 0 \\ 0 & 0 & 0 & \sqrt{\mu_1} & 0 & 0 \\ 0 & 0 & 0 & 0 & \sqrt{\sigma_2} & 0 \\ 0 & 0 & 0 & 0 & 0 & \sqrt{\mu_2} \end{bmatrix} \tag{3.9}$$

The coordinates of the vector $\boldsymbol{v}_e = [z_e, y_e, z_{1e}, y_{1e}, z_{2e}, y_{2e}]^\top_{E_N}$ with respect to the energy basis E_N can be obtained from the vector $\boldsymbol{v}$ with respect to the basis E, using the transition matrix

$$\boldsymbol{v}_e = \mathbf{A}_{E_N \leftarrow E} \boldsymbol{v} \tag{3.10}$$

Then

$$\boldsymbol{v}_e = [\sqrt{\sigma} z, \sqrt{\mu} y, \sqrt{\sigma_1} z_1, \sqrt{\mu_1} y_1, \sqrt{\sigma_2} z_2, \sqrt{\mu_2} y_2]^\top_{E_N} \tag{3.11}$$

The norm of the vector $\boldsymbol{v}_e$ in the energy space with the energy product is as follows

$$\begin{aligned}|\boldsymbol{v}_e| &= \sqrt{\langle \boldsymbol{v}_e, \boldsymbol{v}_e\rangle} = \\ &= \sqrt{\frac{1}{2}[\sqrt{\sigma}(z)^2 + (\sqrt{\mu}y)^2 + (\sqrt{\sigma_1}z_1)^2 + (\sqrt{\mu_1}y_1)^2 + (\sqrt{\sigma_2}z_2)^2 + (\sqrt{\mu_2}y_2)^2]} = \\ &= \sqrt{\frac{\sigma z^2}{2} + \frac{\mu y^2}{2} + \frac{\sigma_1 z_1^2}{2} + \frac{\mu_1 y_1^2}{2} + \frac{\sigma_2 z_2^2}{2} + \frac{\mu_2 y_2^2}{2}} = \\ &= \sqrt{E_p + E_k + E_{p1} + E_{k1} + E_{p2} + E_{k2}}\end{aligned} \tag{3.12}$$

where: E_p is the potential energy accumulated in the spring σ, E_k – kinetic energy of the mass μ, E_{p1} – potential energy accumulated in the spring σ_1, E_{k1} – kinetic energy of the mass μ_1, E_{p2} – potential energy accumulated in the spring σ_2, E_{k2} – kinetic energy of the mass μ_2.

From (3.12) it can be seen that the norm of the vector $\boldsymbol{v}_e$ in the energy space is a square root of the whole energy accumulated in the system.

Using $\mathbf{A}_{E_N \leftarrow E}$, one can find the mathematical model of the system in the transformed space given by the following differential equations

$$\begin{aligned}
&\dot{z}_e = \sqrt{\frac{\sigma}{\mu}}y_e \\
&\dot{y}_e = -\frac{c}{\mu}y_e - \frac{c_1}{\mu}y_e + \frac{c_1}{\sqrt{\mu\mu_1}}y_{1e} - \sqrt{\frac{\sigma}{\mu}}z_e + \sqrt{\frac{\sigma_1}{\mu}}z_{1e} + \frac{F}{\mu}\sin\eta\tau \\
&\dot{z}_{1e} = \sqrt{\frac{\sigma_1}{\mu_1}}y_{1e} - \sqrt{\frac{\sigma_1}{\mu}}y_e \qquad \dot{y}_{1e} = -\sqrt{\frac{\sigma_1}{\mu_1}}z_{1e} - \frac{c_1}{\mu_1}y_{1e} + \frac{c_1}{\sqrt{\mu\mu_1}}y_e \\
&\dot{z}_{2e} = \sqrt{\frac{\sigma_2}{\mu_2}}y_{2e} \qquad \dot{y}_{2e} = -\sqrt{\frac{\sigma_2}{\mu_2}}z_{2e} - \frac{c_2}{\mu_2}y_{2e}
\end{aligned} \tag{3.13}$$

where

$$\begin{aligned}
z_e &= \operatorname{sgn}(x)\sqrt{E_p} & y_e &= \operatorname{sgn}(y)\sqrt{E_k} \\
z_{1e} &= \operatorname{sgn}(x_1)\sqrt{E_{p1}} & y_{1e} &= \operatorname{sgn}(y_1)\sqrt{E_{k1}} \\
z_{2e} &= \operatorname{sgn}(x_2)\sqrt{E_{p2}} & y_{2e} &= \operatorname{sgn}(y_2)\sqrt{E_{k2}}
\end{aligned} \tag{3.14}$$

3.1. Impact map

Let π be the plane determined by the basis vectors (Fig. 4a and Fig. 5)

$$\boldsymbol{b}_{1y} = [0,0,0,(\sqrt{\mu_1})^{-1},0,0]^\top \qquad \boldsymbol{b}_{2y} = [0,0,0,0,0,(\sqrt{\mu_2})^{-1}]^\top \tag{3.15}$$

The co-ordinates y_{1e} and y_{2e}, obtained from y_1 and y_2 with use of $\mathbf{A}_{E_N \leftarrow E}$, correspond to the kinetic energies of the masses μ_1 and μ_2, respectively. The position of the vector is marked on this plane just before and after

the impact. Thus, this plane is a special kind of the impact map. In order to make this map clearer, only half of the points are shown.

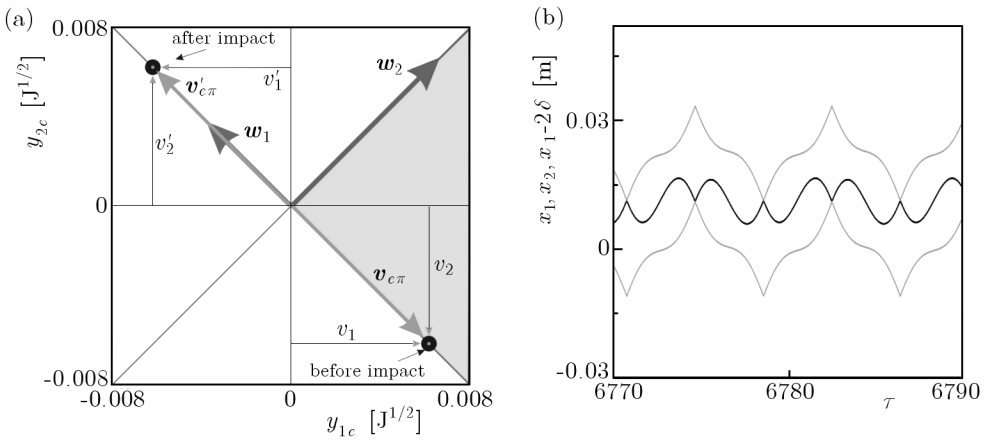

Fig. 4. The impact map and oscillators μ_1 and μ_2 time displacement diagrams; $\varphi = 3\,\text{rad}$, $\eta = 0.92$, $\mu = 1\,\text{kg}$, $\mu_1 = \mu_2 = 0.5\,\text{kg}$, $\sigma = 1\,\text{N/m}$, $\sigma_1 = \sigma_2 = 0.78\,\text{N/m}$, $c = 0.04\,\text{Ns/m}$, $c_1 = c_2 = 0.025\,\text{Ns/m}$, $F = 0.01\,\text{N}$, $\delta = 0.0223\,\text{m}$, $r = 1$, $\Theta = 0.932$

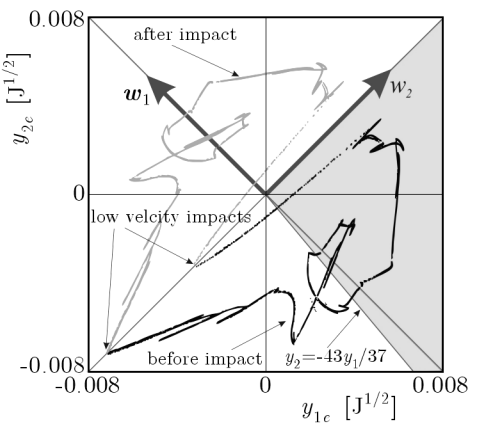

Fig. 5. The impact map; $\eta = 1.23$, $\mu = 1\,\text{kg}$, $\mu_1 = \mu_2 = 0.5\,\text{kg}$, $\sigma = 1\,\text{N/m}$, $\sigma_1 = \sigma_2 = 0.78\,\text{N/m}$, $c = 0.04\,\text{Ns/m}$, $c_1 = c_2 = 0.025\,\text{Ns/m}$, $F = 0.01\,\text{N}$, $\delta = 0.0223\,\text{m}$, $r = 0.85$, $\varphi = 0$, $\Theta = 0.1926$

As the choice criterion

$$y_{1e} > y_{2e} \tag{3.16}$$

has been applied. Thanks to this simplification, the before and after impact parts of the map are separated, and the changes of the vectors during the each impact can be clearly seen.

The consideration of the position and the norm of the vector on this map allows us to conclude about the energy flow between the dynamical and impact absorbers and also about the energy dissipation during each collision. The energy dissipation is introduced into the mathematical model of the system over the restitution coefficient r.

Let us take into consideration vectors in the energy space just before and after the impact and denote them $\boldsymbol{v}_e$ and bmv'_e, respectively. Let $\boldsymbol{v}_{e\pi}$ and $bmv'_{e\pi}$ be the projections of the $\boldsymbol{v}_e$ and $\boldsymbol{v}'_e$ on the plane π, correspondingly (Fig. 4a).

To obtain the transformation of the vector $\boldsymbol{v}_{e\pi}$ during the impact, one can use the Newton impact criterion and the momentum equation. But these are laws that can be applied in the phase space only. Thus, to obtain this transformation, we have to consider it in three stages.

1. The first one is a transformation from the energy to phase space.

   Let us denote this energy subspace transformation as $(\mathbf{A}^{\pi}_{E_N\leftarrow E})^{-1}$:

   $$\boldsymbol{v} = (\mathbf{A}^{\pi}_{E_N\leftarrow E})^{-1}\boldsymbol{v}_{e\pi}$$

   The transformation $(\mathbf{A}^{\pi}_{E_N\leftarrow E})^{-1}$ is always possible because of the linearity of the transformation $\mathbf{A}_{E_N\leftarrow E}$ and the same dimension of the phase and energy space.

2. The second transformation stage consists ofimplementation of the physical laws modelling the impact:

   — The momentum equation

   $$\mu_1 u_1 + \mu_2 u_2 = \mu_1 u'_1 + \mu_2 u'_2 \tag{3.17}$$

   — The Newton equation

   $$u'_1 - u'_2 = -r(u_1 - u_2) \tag{3.18}$$

   where

   $$\boldsymbol{v} = [u_1, u_2] \qquad \boldsymbol{v}' = [u'_1, u'_2]$$

   are velocities of μ_1 and μ_2 before and after the impact, respectively.

   This transformation stage can be described by

   $$\mathbf{A}_{E_N} = \begin{bmatrix} \dfrac{\mu - r}{\mu + 1} & \dfrac{1 + r}{\mu + 1} \\ \dfrac{\mu + \mu r}{\mu + 1} & \dfrac{1 - \mu r}{\mu + 1} \end{bmatrix} \tag{3.19}$$

where

$$\mu = \frac{\mu_1}{\mu_2}$$

and r is the restitution coefficient.

Then

$$\boldsymbol{v}' = \mathbf{A}_{E_N} = \boldsymbol{v} \tag{3.20}$$

3. The third transformation stage is a return from the phase to energy space with use of the transformation $\mathbf{A}_{E_N \leftarrow E}$

$$\boldsymbol{v}'_{e\pi} = (\mathbf{A}^{\pi}_{E_N \leftarrow E})\boldsymbol{v}' \tag{3.21}$$

Finally

$$\boldsymbol{v}'_{e\pi} = (\mathbf{A}^{\pi}_{E_N \leftarrow E})\mathbf{A}_{E_N}(\mathbf{A}^{\pi}_{E_N \leftarrow E})^{-1}\boldsymbol{v}_e \tag{3.22}$$

There exists a case when the transformations of the vector in the phase and energy space are the same. When $\mu_1 = \mu_2$, then

$$\begin{aligned}(\mathbf{A}^{\pi}_{E_N \leftarrow E}) &= \begin{bmatrix}\mu_1 & 0\\ 0 & \mu_1\end{bmatrix} = \mu_1 \begin{bmatrix}1 & 0\\ 0 & 1\end{bmatrix}\\ (\mathbf{A}^{\pi}_{E_N \leftarrow E})^{-1} &= \begin{bmatrix}\mu_1 & 0\\ 0 & \mu_1\end{bmatrix}^{-1} = \frac{1}{\mu_1}\begin{bmatrix}1 & 0\\ 0 & 1\end{bmatrix}\end{aligned} \tag{3.23}$$

and finally

$$\boldsymbol{v}'_{e\pi} = \mathbf{A}_{E_N}\boldsymbol{v}_e \tag{3.24}$$

It means that the transformations of the vectors during the impact in the phase and energy space are the same. In that case, the transformation during the impact can be considered without the first and third stages. The vector transformation is described by $\mathbf{A}_{E_N}$ then.

In that case, the transformation during the impact is

$$\mathbf{A}_{E_N} = \begin{bmatrix}\dfrac{\mu - r}{\mu + 1} & \dfrac{1 + r}{\mu + 1}\\ \dfrac{\mu + \mu r}{\mu + 1} & \dfrac{1 - \mu r}{\mu + 1}\end{bmatrix} \tag{3.25}$$

The eigenvalues of the $\mathbf{A}_{E_N}$ matrix are

$$\lambda_1 = -r\lambda_2 = 1 \tag{3.26}$$

and the corresponding eigenvectors

$$\boldsymbol{w}_1 = \left[\frac{-1}{\mu}, 1\right]^\top \qquad \boldsymbol{w}_2 = [1,1]^\top \tag{3.27}$$

respectively.

The directions of the eigenvectors are shown in Fig. 4a and Fig. 5. Note that during the impact, the vector $\boldsymbol{v}_{e\pi}$ is transformed only along the direction given by the eigenvector $\boldsymbol{w}_1$.

3.2. Energy flow, dissipation and synchronization

The energy dissipation in time of each collision can be found from the change of the norm of the energy space vector

$$|\boldsymbol{v}_{e\pi}| - |\boldsymbol{v}'_{e\pi}| \tag{3.28}$$

The maximum dissipation of the energy takes place when the vector $\boldsymbol{v}_{e\pi}$ has the same direction as the eigenvector $\boldsymbol{w}_1$. Then

$$\boldsymbol{v}'_{e\pi} = \lambda_1 \boldsymbol{v}_{e\pi} \tag{3.29}$$

Taking in the consideration that

$$|\boldsymbol{v}_{e\pi}| = \sqrt{E_{K1} + E_{K2}} \tag{3.30}$$

where: E_{K1}, E_{K2} – kinetic energy of the mass μ_1 and μ_2 before the impact, respectively, and

$$|\boldsymbol{v}'_{e\pi}| = \sqrt{E'_{K1} + E'_{K2}} \tag{3.31}$$

where: E'_{K1}, E'_{K2} – kinetic energy of the mass μ_1 and μ_2 after the impact.

After substituting Eqs. (3.30) and (3.31) into Eq. (3.29), it can be found that the energy relation after and before the impact assumes the form

$$\frac{E'_{K1} + E'_{K2}}{E_{K1} + E_{K2}} = \lambda_1^2 = r^2 \tag{3.32}$$

The closer the direction of the vector $\boldsymbol{v}_{e\pi}$ is to the second eigenvector $\boldsymbol{w}_2$, the less energy dissipation occurs. In the case when the directions of $\boldsymbol{v}_{e\pi}$ and $\boldsymbol{w}_2$ are almost the same, there is almost no energy dissipation during the collision. The velocities of the oscillators μ_1 and μ_2 are almost equal then, and in practice a small disturbance can cause that the impact occurs or not. It is the so-called grazing collision and it causes chaotic motion of the system.

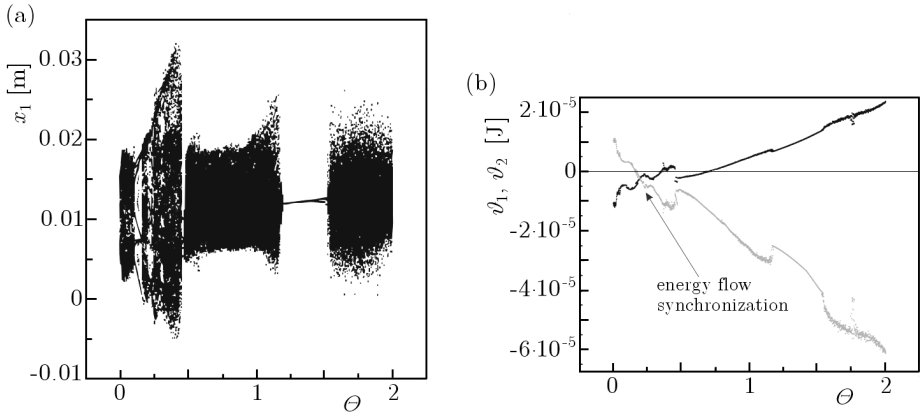

Fig. 6. (a) $x1$Bbifurcation diagram, (b) Reduced Inertia Moment bifurcation diagram; $\eta = 1.23$, $\mu = 1\,\mathrm{kg}$, $\mu_1 = \mu_2 = 0.5\,\mathrm{kg}$, $\sigma = 1\,\mathrm{N/m}$, $\sigma_1 = \sigma_2 = 0.78\,\mathrm{N/m}$, $c = 0.04\,\mathrm{Ns/m}$, $c_1 = c_2 = 0.025\,\mathrm{Ns/m}$, $F = 0.01\,\mathrm{N}$, $\delta = 0.0223\,\mathrm{m}$, $r = 0.85$, $\varphi = 0$

These special points can be seen in Figs. 2, 4 and Fig. 6a as common points of the before and after impact attractors. Such points can be observed in the time dependence chart in Fig. 6b as well.

The transformation matrix $\mathbf{A}_{E_N}$ allows one also to divide the impact map into two kinds of fields: the first one for the case when the energy flows during the impact from the dynamical to impact absorber and the second one when the energy flows in the opposite direction.

Consider the matrix $\mathbf{A}_{E_N}$ in the case $\mu_1 = \mu_2$

$$\mathbf{A}_{E_N} = \begin{bmatrix} \dfrac{1-r}{2} & \dfrac{1+r}{2} \\ \dfrac{1+r}{2} & \dfrac{1-r}{2} \end{bmatrix} \tag{3.33}$$

Let

$$\boldsymbol{v}_{e\pi} = [v_1, v_2]^\top \qquad \boldsymbol{v}'_{e\pi} = [v'_1, v'_2]^\top \tag{3.34}$$

Then

$$\boldsymbol{v}'_{e\pi} = \mathbf{A}_{EN}\boldsymbol{v}_{e\pi} \tag{3.35}$$

so

$$\begin{bmatrix} v'_1 \\ v'_2 \end{bmatrix} = \begin{bmatrix} \dfrac{1-r}{2} & \dfrac{1+r}{2} \\ \dfrac{1+r}{2} & \dfrac{1-r}{2} \end{bmatrix} \begin{bmatrix} v_1 \\ v_2 \end{bmatrix} \tag{3.36}$$

The energy flow from the dynamical to impact absorber is given by the condition

$$|v_1'| \leqslant |v_1| \tag{3.37}$$

or the equivalent

$$-v_1 \leqslant v_1' \leqslant v_1 \tag{3.38}$$

Consider:

1. $v_1' = v_1$

   The condition is satisfied when the directions of $\boldsymbol{v}_{e\pi}$ and the eigenvector $\boldsymbol{w}_2$ are the same.

2. $v_1' = -v_1$

   Then

$$-v_1 = \frac{1-r}{2}v_1 + \frac{1+r}{2}v_2 \tag{3.39}$$

   and we obtain

$$v_2 = -\frac{3-r}{1+r}v_1 \tag{3.40}$$

   For the case shown in Fig. 5, $r = 0.85$ and then

$$v_2 = -\frac{43}{37}v_1 \tag{3.41}$$

   As a result, the energy flow from the dynamical to impact absorber occurs:

   — if $v_1 > 0$

$$-\frac{43}{37}v_1 \leqslant v_2 \leqslant v_1 \tag{3.42}$$

   — if $v_1 < 0$

$$v_1 \leqslant v_2 \leqslant -\frac{43}{37}v_1 \tag{3.43}$$

The field of the energy flow along this direction is marked in Fig. 2 in grey. Note that it is just for y1e ¿ y2e, which was the criterion of the impact choice, see Eq. (3.16). As can be seen, during the impacts in the case under consideration, the energy flows in both directions. The amount of energy that flows in each direction can be quantified with use of the coefficients ϑ_1 and ϑ_2 introduced below.

One can also treat the energy flow during each impact as a change of the inertia moment of the map before and after the impact.

Consider the coordinates v_1, v_2 and v_1', v_2' of the vectors before and after the impact (see Fig. 4). From the structure of the energy space, the kinetic energies E_{k1} and E_{k2} of the dynamical and impact absorber are, respectively

$$\begin{aligned} v_1^2 &= E_{K1} & v_2^2 &= E_{K2} \\ {v_1'}^2 &= E'_{K1} & {v_2'}^2 &= E'_{K2} \end{aligned} \tag{3.44}$$

From Eqs. (3.44) and Fig. 4, it can be seen that these energies are equal to the inertia moments of the considered point against the respective axis.

Thus, the energy changes in time of each impact along the directions of y_{1e} and y_{2e}

$$\begin{aligned} \Delta E_{K1} &= E'_{K1} - E_{K1} = {v_1'}^2 - v_1^2 \\ \Delta E_{K2} &= E'_{K2} - E_{K2} = {v_2'}^2 - v_2^2 \end{aligned} \tag{3.45}$$

Considering all the n impacts on the map sums of the energy changes ΔE_{K1} and ΔE_{K2}

$$\begin{aligned} \sum \Delta E_{K1} &= \sum (E'_{K1} - E_{K1}) = \sum ({v_1'}^2 - v_1^2) \\ \sum \Delta E_{K2} &= \sum (E'_{K2} - E_{K2}) = \sum ({v_2'}^2 - v_2^2) \end{aligned} \tag{3.46}$$

and denoting the inertia moments of the before and after impact parts of the map as

$$\begin{aligned} \sum {v_1'}^2 &= I_1' & \sum v_1^2 &= I_1 \\ \sum {v_2'}^2 &= I_2' & \sum v_2^2 &= I_2 \end{aligned} \tag{3.47}$$

the energy that has flown between the dynamical and impact absorber during all the impacts can be treated as a change of the inertia moments of the whole map as regards the respective axis

$$\sum \Delta E_{K1} = I_1' - I_1 \qquad \sum \Delta E_{K2} = I_2' - I_2 \tag{3.48}$$

The energy changes during each of n impacts can be considered as the average amount of the energy that flows during one impact

$$\frac{\sum \Delta E_{K1}}{n} = \frac{I_1' - I_1}{n} = \vartheta_1 \qquad \frac{\sum \Delta E_{K2}}{n} = \frac{I_2' - I_2}{n} = \vartheta_2 \tag{3.49}$$

and the energy flow criterion formulated as $\vartheta_1 > \vartheta_2$ for the flow from the dynamical to impact absorber, and $\vartheta_1 < \vartheta_2$ for the flow in the opposite direction.

On the basis of the ϑ_1 and ϑ_2, a synchronization index can be introduced

$$\zeta = \vartheta_1 - \vartheta_2$$

Note that the condition $\zeta > 0_2$ is equivalent to $\vartheta_1 > \vartheta_2$ and $\zeta < 0_2$ is equivalent to $\vartheta_1 < \vartheta_2$.

In consequence, its zero value represents the energy synchronization state, where on average the same amount of energy flows between the systems in both the directions. This index was applied in searching for the energy flow synchronization with use of the ANN.

Changes in the energy flow depending on the system parameter Θ, where

$$\Theta = \frac{F}{F_2} \tag{3.50}$$

are shown in Fig. 6. The system parameter set was chosen in such a way that the behaviour of parameters ϑ_1 and ϑ_2 for different types of the system dynamics can be observed. One can see the regions where the energy flows from the dynamical to impact absorber $\vartheta_1 > \vartheta_2$ and in the opposite direction, when the ϑ_1 curve lies under the ϑ_2 curve. What is important, even though there exist chaotic regions, which can be seen in the bifurcation diagram in Fig. 6a, the energy flow coefficients ϑ_1, ϑ_2 behave very stable. Their changes in the regions of the bifurcation points can be observed as well. Thus, not only a local impact dynamics can be controlled with use of them, but also the global system behaviour.

It is also advantageous to consider the ϑ_1 and ϑ_2 curve intersection point. Such a point appears when the average amount of the energy that flows out/into the coupled systems is the same. It can be seen in Fig. 6 and Fig. 7. These cases are chosen to illustrate different types of the energy flow synchronization.

The first one, presented in Fig. 6, shows the chaotic energy flow synchronization point as a transition point between the flow of energy from the dynamical to impact absorber and the flow in the opposite direction. Such a point lies under the horizontal axis, which means a loss of energy of both the coupled systems. This energy is dissipated during the impacts. An impact map for this synchronization point is depicted in Fig. 5. One can see the points that lie along the eigenvector $\boldsymbol{w}_2$ direction, showing low velocity impacts that cause the chaotic dynamics.

In Fig. 7, the next three synchronization points are presented. An impact map and a time displacement diagram for the first of them are shown in Fig. 8. One can see in Fig. 8a that the before and after impact attractors osculate each

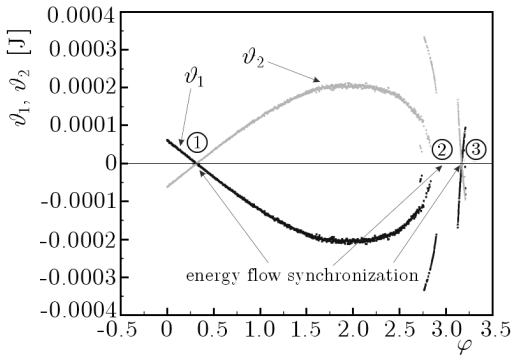

Fig. 7. (The Reduced Inertia Moment bifurcation diagram; $\eta = 0.92$, $\mu = 1\,\mathrm{kg}$, $\mu_1 = \mu_2 = 0.5\,\mathrm{kg}$, $\sigma = 1\,\mathrm{N/m}$, $\sigma_1 = \sigma_2 = 0.78\,\mathrm{N/m}$, $c = 0.04\,\mathrm{Ns/m}$, $c_1 = c_2 = 0.025\,\mathrm{Ns/m}$, $F = 0.01\,\mathrm{N}$, $\delta = 0.0223\,\mathrm{m}$, $r = 1$, $\Theta = 0.932$

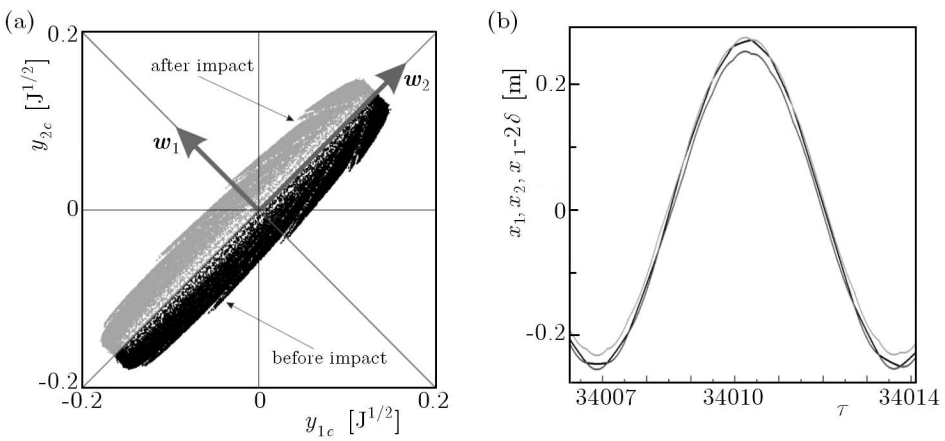

Fig. 8. Synchronization point no. 1; (a) the impact map, (b) oscilators μ_1 and μ_2 time displacement diagrams; $\varphi = 0.316\,\mathrm{rad}$, $\eta = 0.92$, $\mu = 1\,\mathrm{kg}$, $\mu_1 = \mu_2 = 0.5\,\mathrm{kg}$, $\sigma = 1\,\mathrm{N/m}$, $\sigma_1 = \sigma_2 = 0.78\,\mathrm{N/m}$, $c = 0.04\,\mathrm{Ns/m}$, $c_1 = c_2 = 0.025\,\mathrm{Ns/m}$, $F = 0.01\,\mathrm{N}$, $\delta = 0.0223\,\mathrm{m}$, $r = 1$, $\Theta = 0.932$

other along the direction of $\boldsymbol{w}_1$. It means that there are numerous low velocity impact points. They can be seen in the time dependent chart in Fig. 8b.

Figure 9 depicts the next synchronization point in the case of impactless motion and no energy flow between the systems.

The synchronization point shown in Fig. 4 represents the periodic energy flow synchronization. This point is presented only to clear up all the presented cases and analysis. The presented behaviour is possible only theoretically

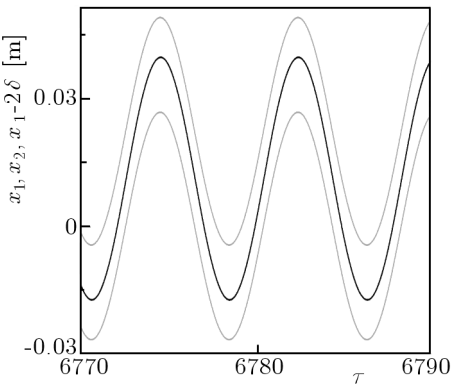

Fig. 9. Synchronization point no. 2; oscilators μ_1 and μ_2 time displacement diagrams; $\varphi = 3\,\text{rad}$, $\eta = 0.92$, $\mu = 1\,\text{kg}$, $\mu_1 = \mu_2 = 0.5\,\text{kg}$, $\sigma = 1\,\text{N/m}$, $\sigma_1 = \sigma_2 = 0.78\,\text{N/m}$, $c = 0.04\,\text{Ns/m}$, $c_1 = c_2 = 0.025\,\text{Ns/m}$, $F = 0.01\,\text{N}$, $\delta = 0.0223\,\text{m}$, $r = 1$, $\Theta = 0.932$

because the restitution coefficient r value equals 1. In such a case, the eigenvalue λ_1 introduced in Eq. (3.26)

$$\lambda_1 = -1 \tag{3.51}$$

Taking into the consideration the second eigenvalue

$$\lambda_2 = 1 \tag{3.52}$$

(see Eq. (3.26)) it can be concluded that the transformation during the impacts is very particular. First, let us note that the points lie on the grey region border, introduced in Eqs. (3.37)-(3.43). This border divides the map into parts of the energy flowing out and into the coupled system. This border position of the considered points means that during the impacts the energy neither flows to the dynamic absorber nor to the impact absorber. The impacts are symmetrical, which one can see in Fig. 8b. According to Eqs. (3.51) and (3.52), the points only jump from one part of the map to the second one and back from the second to the first one. Norms of the vectors during transformations do not change, which means no energy dissipation during the impacts.

3.3. Neural network predictions of the systems synchronization

The task for the neural network was to solve a prediction problem of the synchronization index ζ for the given system parameters. An approximation of the teaching function is presented in Fig. 9.

The synchronization index

$$\zeta = \vartheta_1 - \vartheta_2$$

shows the energy flow direction between colliding systems. In consequence, its zero value represents the energy synchronization state, where on average the same amount of energy flows between the systems in both directions. For a teaching set, the system parameters r and Θ were considered (Fig. 2). One can see a set of bifurcation diagrams in it. Each line represents one bifurcation diagram and shows the direction of the system parameter changes. Note that unlike the traditional bifurcation diagrams, two system parameters are changed at the same time. Thanks to that, it is possible to prepare a set of dispersed data representing the system dynamics with slightly tuning of the system parameters without introducing disturbances causing unstable motions, or jumping between coexisting attractors. Preparation of the teaching set was made in Delphi, with the Runge-Kutta method applied to integrate the differential equation set. An approximation of the teaching set is presented in Fig. 10. Then, the teaching set was entered into the Statistica Neural Network software. On the input of the ANN, the parameters r and Θ were given, and on the output – the index ζ. After the teaching procedure, such a network can approximate the index ζ values for the ranges of the parameters r and Θ that were not introduced to the ANN during the teaching process. It allows one to find the system control index for the whole system parameter range. To find the desired control index value output, neural network values were examined. In the case under consideration, the desired control index value represents the energy flow synchronization phenomena of the coupled systems.

In the neural network type searching process, three-layer MLP and RBF nonlinear networks were considered. The RBF-type network could not solve the task, even though a very complex hidden layer topology was considered. For the MLP network, the teaching process was much more efficient. In the cases under consideration, an aggregation function of all neurons was linear. The best results of the teaching process were obtained for hyperbolic tangent activation functions of the hidden and third layer neurons.

As a result, a three-layer network with two inputs, one thousand neurons in the hidden layer and one output, was obtained.

A comparison of this neural network prediction and numerical simulations are shown in Fig. 11. One can see a good convergence of these results. And what is important, the results are accurate very much in the zero neighbourhood, which is a synchronization point.

Neural networks taught in such a way can be now used in dynamical system investigations. A set of system parameters can be entered in the neural

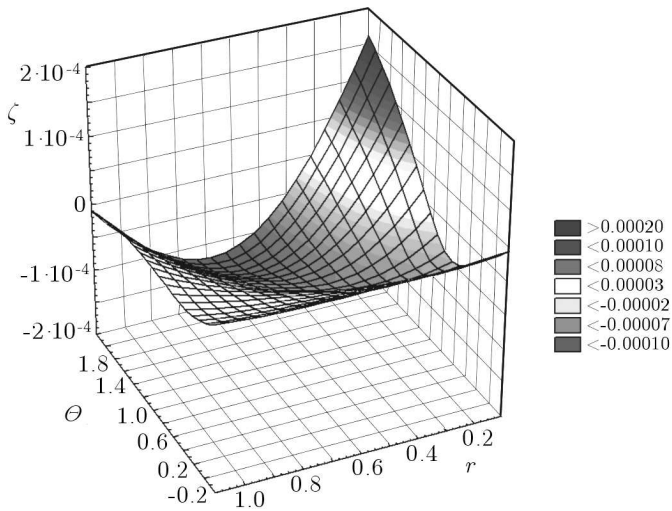

Fig. 10. An approximation of the teaching fuction; the input : r, Θ, output: ζ [J]

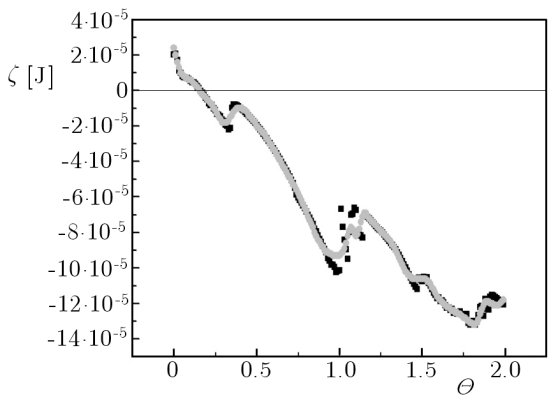

Fig. 11. Comparison of simulations (black) and neural network prediction of the synchronization parameter ζ depending on the parameter Θ; $\eta = 1.23$, $\mu = 1\,\mathrm{kg}$, $\mu_1 = \mu_2 = 0.5\,\mathrm{kg}$, $\sigma = 1\,\mathrm{N/m}$, $\sigma_1 = \sigma_2 = 0.78\,\mathrm{N/m}$, $c = 0.04\,\mathrm{Ns/m}$, $c_1 = c_2 = 0.025\,\mathrm{Ns/m}$, $F = 0.01\,\mathrm{N}$, $\delta = 0.0223\,\mathrm{m}$, $r = 0.85$, $\varphi = 0$

network input and values of the energy parameters will be obtained. In the case one is interested in a given value of the output parameter, for instance, the synchronization zero value, a numerical algorithm has to be developed to find out the interesting parameters from the neural network answer. Examples of such predictions obtained from the algorithm written in Delphi are shown in Fig. 12. From the neural network output values, the algorithm chooses values that belong to the ε range.

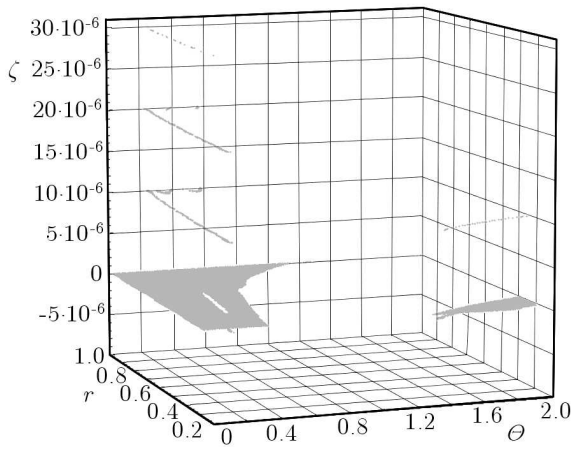

Fig. 12. The neural network prediction of the synchronization parameter ζ depending on r and Θ parameters

In the case of the monotonous dependence between the input and the output, the problem of searching the accurate index value can be simplified. It can be formulated in the inverse direction and the neural network can be taught to provide the parameters under interest as the input during the teaching process, and then, the respective system coefficients.

4. Conclusions

A structure and an application of the Impact Map supported with Artificial Neural Networks in the energy flow and the synchronization analysis were described. This structure applies an idea of the Energy Vector Space in the system with impacts. A transformation of the traditional phase space into the energy space was shown and a structure of the energy map was presented. This structure was applied to investigate and recognize the energy flow, dissipation and synchronization. Energy flow direction changes with synchronization as a transitional state were shown. Different types of the energy flow synchronization were analyzed. The results of numerical simulations were used in the neural network teaching process. A comparison of the results of the straight impact map simulation and the neural network prediction was conducted. The system index prediction for the energy flow synchronization state with use of the neural network was presented. A new type of the index allowing one to control the system dynamic state was introduced. It was shown that it was

connected with the behaviour of the system and allowed one to find different types of the system dynamics. It enables recognizing energy flow directions and energy flow synchronization. It was demonstrated that even for chaotic regions, it behaved very stable. It was shown that the proposed method allowed us to predict the system behaviour, and also enabled searching for the particular system behaviour. One could see that the index was changing in the regions of bifurcations. Thus, with use of this index, not only local impact dynamics, but also the global system behaviour can be controlled.

References

1. AIDANPAA J.O., GUPTA R.B., 1993, Periodic and chaotic behaviour of a threshold-limited two-degree-of-freedom system, *Journal of Sound and Vibration*, **165**, 2, 305-327
2. ASTAKHOV V., KAPITANIAK T., SHABUNIN A., ANISHCHENKO V., 1999, Non-bifurcational mechanism of loss of chaos synchronization in coupled nonidentical systems, *Physic Letters A*, **258**, 99-102
3. BANKOVSKIV N.G., KOROTKOV K.G., PETROV N.N., 1986, Physical image-forming processes in gas-discharge visualisation (the Kirlian effect)(review), *Soviet Journal of Communications and Technology*, **31**, 29-45
4. BLEKHMAN II, 1988, *Synchronization in Science and Technology*, ASME Press, New York
5. BŁAŻEJCZYK-OKOLEWSKA B., BRINDLEY J., CZOŁCZYŃSKI K., KAPITANIAK T., 2001, Antiphase Synchronization of chaos by noncontinuous coupling: two impacting oscillators, *Chaos, Solitons & Fractals*, **12**, 1823-1826
6. BŁAŻEJCZYK-OKOLEWSKA B., CZOŁCZYŃSKI K., KAPITANIAK T., 2007, Dynamics of a two-degree-of-freedom cantilever beam with impacts, *Chaos, Solitons & Fractals*, doi:10.1016/j.chaos.2007.09.097
7. CHEN G., DONG X., 1998, *From Chaos to Order*, World Scientific, Singapore
8. CZOŁCZYŃSKI K., 2001, On the existence of a stable periodic motion of two impacting oscillators, *Chaos, Solitons & Fractals*, **15**, 371-379
9. CZOŁCZYŃSKI K., PERLIKOWSKI P., STEFAŃSKI A., KAPITANIAK T., 2009, Clustering and synchronization of n Huygens' clocks, *Physica A*, **338**, 5013-5023
10. DĄBROWSKI A., 2000, New design of the impact damper, *Mechanics and Mechanical Engineering*, **4**, 2, 191-196
11. DĄBROWSKI A., 2005, The construction of the energy space, *Chaos, Solitons & Fractals*, **26**, 1277-292

12. Dąbrowski A., 2007, Application of the energy space in chaotic systems research, *Mechanics and Mechanical Engineering*, **11**, 1, 21-36

13. Dąbrowski A., 2009, Energy-Vector Method in mechanical oscillations, *Chaos, Solitons & Fractals*, **39**, 1684-1697

14. Dąbrowski A., Kapitaniak T., 2001, Using chaos to reduce oscillations, *Nonlinear Phenomena in Complex Systems*, **4**, 2, 206-211

15. Dąbrowski A., Kapitaniak T., 2009, Using chaos to reduce oscillations: experimental results, *Chaos, Solitons & Fractals*, **39**,1677-1683

16. Duch W., Korbicz J., Rutkowski L., Tadeusiewicz R., 2000, *Sieci neuronowe*, **6**, AOW Exit [in Polish]

17. Duch W., Pilichowski M., 2007, Experiments with computational creativity, *Neural Information Processing – Letters and Reviews*, **11**, 123-133

18. Dudek-Dyduch E., Tadeusiewicz R., Horzyk A., 2009, Neural network adaptation process effectiveness dependent on constatnt training data availability, *Neurocomputing*, **72**, 3138-3149

19. Fries P., Reynolds J., Rorie A., Dismone R., 2001, Modulation of oscillatory neuronal synchronization by selective visual attention, *Science*, **291**, 5508, 1560-1563

20. Gourdon E., Lamarque C.H., 2005, Energy pumping for a larger span of energy, *Journal of Sound and Vibration*, **285**, 3, 711-720

21. Kapitaniak T., 1996, *Controlling Chaos*, Academic Press, London

22. Kapitaniak T., 1998, *Chaos for Engineers*, Springer-Verlag, Berlin, Heidelberg

23. Kapitaniak T., Maistrenko Yu.L., 1998, Chaos synchronization and riddled basins in two coupled one-dimensional maps, *Chaos, Solitons & Fractals*, **9**, 2, 271-282

24. Kapitaniak T., Wiercigroch M., 2000, Dynamics of impact systems, *Chaos, Solitons & Fractals*, **11**, 2411-2412

25. Keane A.J., Price W.G., 1991, A note on the power flowing between two conservatively coupled multi-modal subsystems, *Journal of Sound and Vibration*, **144**, 185-186

26. Kishimoto Y., Bernstein D.S., Hall S.R., 1995, Energy flow modelling of interconnected structures: a deterministic foundation for statistical energy analysis, *Journal of Sound and Vibration* , **183**, 3, 407-445

27. Korotkov K.G., 2002, *Human Energy Field: Study with GDV Bioelectrography*, Backbone Publishing Company, USA

28. Lachaux J.P., Chavez M., Lutz A., 2003, A simple measure of correlation across time, frequency and space between continuous brain signals, *J. Neuroscience Methods*, **123**, 175-188

29. Lachaux J.P., Rodrigues E., Le Van Quyen M., Lutz A., Martinerie J., Varela F., 2000, Studying single-trials of phase synchronous activity in the brain, *Int. J. Bifurcat. Chaos*, **10**, 10, 2429-2439

30. Lee J.-Y., Yan J.-J., 2006, Control of impact oscillator, *Chaos, Solitons & Fractals*, **28**, 136-142

31. Lindner B., Schimansky-Geier L., 2000, Coherence and stochastic resonance in a two-state system, *Phys. Rev. E*, **61**, 6103-6110

32. Ma Y., Ing J., Baneriee S., Wiercigroch M., Pavlowskaja E., 2008, The nature of the normal form map for soft impacting systems, *International Journal of Non-Linear Mechanics*, **43**, 504-513

33. Mace B.R., 1992, Power flow between two continuous one-dimensional subsystems: a wave solution., *Journal of Sound and Vibration*, **154**, 289-320

34. Mace B.R., 1994, The statistical energy analysis of two continuous one-dimensional subsystems, *Journal of Sound and Vibration*, **166**, 429-461

35. Maidanik G., Becker K.J., 2003, Dependence of the induced loss factor on the coupling forms and coupling strengths: energy analysis, *Journal of Sound and Vibration*, **266**, 33-48

36. Markiewicz T., Ossowski S., 2005, OLS versus SVM approach to learning of RBF networks, *IJCNN Montreal*, 1051-1056

37. Nichols J.M., Moniz L., Nichols J.D., Pecora L.M., Cooch E., 2007, Assessing spatial coupling in complex population dynamics using mutal prediction and continuity statistics, *Physic Letters A*, **371**, 48-57

38. Ogiela M.R., Tadeusiewicz R., Ogiela L., 2006, Image languages in intelligent radiological palm diagnostics, *Pattern Recognition*, **39**, 2157-2165

39. Ogiela L., Tadeusiewicz R., Ogiela M.R., 2008, Cognitive techniques in medical information systems, *Computers in Biology and Medicine*, **38**, 501-507

40. Ossowski S., Tran L.H., Budzewski K., 2004, Neuro-fuzzy TSK network for calibration of semiconductor sensor array for gas measurements, *IEEE Trans. on Measurements*, **53**, 330-337

41. Ossowski S., Tran L.H., Markiewicz T., 2005, Recognition of the heartbeats using support vector machine networks – a comparitive study, *Lecture Notes on Computer Science*, **3697**, 637-642

42. Pecora L.M., Carroll T.L., Johnson G.A., Mar D.J., Heagy J.F., 1997, Fundamentals of synchronization in chaotic systems, concepts and applications, *Chaos*, **7**, 520-543

43. Pennestri E., 1998, An application of Chebyshev's min-max criterion to the optimal design of a damped dynamic vibration absorber, *Journal of Sound and Vibration*, **217**, 757-765

44. Peterka F., 1970, An investigation of the motion of impact dampers: theory of the fundamental impact motion, *Strojnicky Casopis*, **21**, 5, 457-78

45. Peterka F., Vacik J., 1992, Transition to chaotic motion in mechanical systems with impacts, *Journal of Sound and Vibration*, **154**, 1, 95-115

46. Rodrigues E., George N., Lachaux J.P., Martinerie J., Renault B., Varela F., 1999, Perception's shadow: long distance synchronization of human brain activity, *Nature*, **397**, 430-433

47. Sado D., 1992, *Przenoszenie energii w nieliniowo sprzężonych układach o dwóch stopniach swobody*, Politechnika Warszawska, Warszawa [in Polish]

48. Shu Y., Zhang A., Tang B., 2005, Switching among three different kinds of synchronization for delay chaotic systems, *Chaos, Solitons & Fractals*, **23**, 2, 563-571

49. Stefański A., 2004, *Estymacja maksymalnego wykładnika Lapunowa układów dynamicznych w oparciu o zjawisko synchronizacji*, Praca Habilitacyjna, Politechnika Łódzka, Zeszyty Naukowe Nr 941 [in Polish]

50. Stefański A., Dąbrowski A., Kapitaniak T., 2005, Evaluation of the largest Lyapunov exponent in dynamical systems with time delay, *Chaos, Solitons and Fractals*, **23**, 1651-1659

51. Szaleniec M., Tadeusiewicz R., Witko M., 2008, How to select an optimal neural model of chemical reactivity?, *Neurocomputing*, **72**, 241-256

52. Tadeusiewicz R., Ogiela L., Ogiela M.R., 2008, The automatic understanding approach to system analysis and design, *International Journal of Information Management*, **28**, 38-48

53. Tadeusiewicz R., Ogiela M.R., 2004, *Medical Image Understanding Technology*, Spriger, Berlin, Heidelberg

54. Tsakirtzis S., Kerschen G., Panagopoulos P.N., Vakakis A.F., 2005, Multi-frequency nonlinear energy transfer from linear oscillators to mdof essentially nonlinear attachments, *Journal of Sound and Vibration*, **285**, 1/2, 483-490

55. Xu H.D., Lee H.P., Lu C., 2004, Numerical study on energy transmission for rotating hard disk systems by structural intensity technique, *International Journal of Technical Sciences*, **46**, 639-652

56. Yamaguchi A., Watanabe H., Mikami S., Wada M., 1999, Characterization of biological internal dynamics by the synchronization of coupled chaotic system, *Robotic and Astronomous Systems*, **28**, 195-206

57. YAMPI R., BOCCALETTI S., ANISHCHENKO V., 2007, Active control of the synchronization manifold in a ring of mutually coupled oscillators, *Physic Letters A*, **371**, 48-57

58. ZHANG J., SUN J., 2004, Automatic classification of MRI images for three dimensional volume reconstructure by using general regression neural networks, *Conference Rec. IEE Nucl. Sci. Symp.*, **5**, 3188-3189

Aplikacje sztucznych sieci neuronowych w badaniach parametrycznych przepływu i synchronizacji energii

Streszczenie

Dynamika układów nieliniowych jest bardzo skomplikowanym zagadnieniem z wieloma aspektami wciąż pozostającymi bez rozwiązania. Do badań takich układów stosuje się wiele różnych metod. Wnikliwa analiza związana jest najczęściej z bardzo czasochłonnymi symulacjami numerycznymi. Istnieje w związku z tym duże zapotrzebowanie na opracowanie metod upraszczających ten proces.

W artykule pokazano zastosowanie sztucznych sieci neuronowych (ANN) wspomagających badania przepływu i synchronizacji energii. W badaniach zastosowano Mapy Uderzeń, będące efektem przedstawienia dynamiki układu z uderzeniami w przestrzeni energetyczno-wektorowej. Pokazano zmiany przepływu energii z przejściowym stanem synchronizacji. Wprowadzono nowy rodzaj parametru pozwalającego na określanie stanu dynamicznego układu z uderzeniami. Wyniki przeprowadzonych symulacji numerycznych zostały wykorzystane w procesie uczenia sztucznej sieci neuronowej. Przedstawiono następnie porównanie wyników symulacji i rozwiązania uzyskanego z sieci neuronowej oraz przewidywania parametrów układu, dla których występuje synchronizacja przepływu energii.

Manuscript received April 12, 2010; accepted for print June 22, 2010